Int J Thermophys (2012) 33:843–863
DOI 10.1007/s10765-012-1184-2

Canadian Field Soils II. Modeling of *Quartz* Occurrence

V. R. Tarnawski · M. L. McCombie · W. H. Leong · B. Wagner · T. Momose · J. Schönenberger

Received: 18 September 2011 / Accepted: 10 March 2012 / Published online: 10 April 2012

Abstract The measured mineral composition data (XRD/XRF) of 40 Canadian soils were modeled for the presence of *quartz* as a function of soil texture. Preliminary modeling revealed a lack of strict correlation between *quartz* content and mass fraction of sand. For that reason, the occurrence of *quartz* content was modeled as dependent on a combined fraction of sand and silt, which produced an improved correlation for all tested soils. Then, all soils were modeled separately for five assigned provinces/regions of Canada and strong correlations of *quartz* versus combined sand and silt fractions were obtained. Estimates of *quartz* content and an average thermal conductivity of other minerals were also obtained by the reverse analysis of the weighted geometric mean model applied to the experimental thermal conductivity data of saturated soils. In general, *quartz* estimates followed XRD/XRF data sufficiently well. The thermal conductivity of the remaining soil minerals was about 2.13 $W \cdot m^{-1} \cdot K^{-1}$ on average and did not depend on the soil texture.

Keywords Canadian soils · Reverse modeling of *quartz* content · Thermal conductivity · XRD/XRF analysis

V. R. Tarnawski (✉) · M. L. McCombie
Saint Mary's University, 923 Robie St., Halifax B3H 3C3, Canada
e-mail: vlodek.tarnawski@smu.ca

W. H. Leong
Ryerson University, 350 Victoria Street, Toronto, ON M5B 2K3, Canada

B. Wagner · T. Momose
Bavarian Environment Agency, Hans-Högn-Straße 12, 95030 Hof/Saale, Germany

J. Schönenberger
Bavarian Environment Agency, Leopoldstraße 30, 95615 Marktredwitz, Germany

1 Introduction

The thermal conductivity of solid phases (λ_s) is a key parameter in the modeling of soil thermal conductivity. Its value strongly depends on the volumetric content of *quartz* (Θ_{qtz}) whose thermal conductivity (λ_{qtz}) is considerably higher than the other soil minerals. *Quartz* is not only the dominant mineral in many rock types, but it is also the dominant phase in the sand and silt fractions of natural soils as it is strongly resistant to chemical and mechanical weathering [1]. A good knowledge of soil mineral composition is essential to obtain reliable estimates of soil thermal conductivity.

Complete soil mineral data of 40 Canadian soils was obtained by a combined use of XRD and XRF techniques [2,3]. The use of these two techniques is rare, due to the need for very expensive hardware and highly qualified personnel. Consequently, reliable Θ_{qtz} data of field soils is uncommon. Up to date, there exists only one set of complete mineral composition data of 19 soils that was obtained using only the XRD technique [4]. Additionally, these data include soils of volcanic origin and shows considerable inconsistency of Θ_{qtz} with soil texture which limits its applicable use. As a result, Peters-Lidard et al. [5] published Θ_{qtz} estimates that were nearly the same as sand mass fractions in soils, but these estimates were never verified in the laboratory. As a result, λ_s is assumed as a fitting parameter in a large majority of predictive models [6–8]. Recently, Tarnawski et al. [9] assessed Θ_{qtz} by the reverse analysis of the geometric mean model applied to experimental soil thermal conductivity data at full saturation (λ_{sat}). This modeling approach produced acceptable results compared to experimental Θ_{qtz} data of 10 soils studied by Lu et al. [10]. This approach requires a more comprehensive verification against measured mineral data. In conclusion, the primary objective of this paper is to carry out reverse modeling of Θ_{qtz} and other remaining minerals and to establish possible correlations between texture and Θ_{qtz} for the 40 Canadian soils.

2 Soil Samples

Laboratory XRD/XRF measurements were performed on the 40 soil samples from nine Canadian provinces [3]; a summary of their mineral composition is given in the Appendix. Their detailed textural characteristics are summarized in Table 1.

Table 1 Canadian soils: basic physical characteristics

Code	Name	ρ_s	Porosity n	Texture	GSD			LOI
					m_{cl}	m_{si}	m_{sa}	
NS-01	Acadia	2.71	0.55	Silt loam	0.10	0.57	0.32	0.056
NS-02	Cumberland	2.71	0.45	Sandy loam	0.05	0.34	0.61	0.025
NS-03	Pugwash	2.68	0.40	Sandy loam	0.05	0.37	0.57	0.029
NS-04	Sable sand	2.66	0.36	Sand	0.00	0.00	1.00	0.001
NS-05	Cornwallis-Annapolis-V	2.66	0.40	Loamy Sand	0.03	0.13	0.85	0.038
NS-06	Pugwash - Annapolis-V	2.68	0.51	Sandy Loam	0.06	0.38	0.56	0.050

Table 1 continued

Code	Name	ρ_s	Porosity n	Texture	GSD m_{cl}	m_{si}	m_{sa}	LOI
NS-07	Queens - Annapolis-V	2.78	0.57	Silt Loam	0.12	0.67	0.22	0.068
PE-01	PE1	2.64	0.44	Loam	0.08	0.42	0.50	0.052
PE-02	PE2	2.66	0.42	Loam	0.09	0.39	0.51	0.042
PE-03	PE3	2.66	0.41	Loamy sand	0.03	0.14	0.83	0.026
NB-01	Caribou	2.59	0.54	Silt loam	0.15	0.82	0.03	0.077
NB-02	Victoria	2.54	0.56	Silt loam	0.17	0.83	0.00	0.105
NB-03	Juniper	2.57	0.62	Silt loam	0.10	0.66	0.24	0.120
NB-04	Queens	2.59	0.54	Silt loam	0.10	0.64	0.26	0.090
NB-05	Fundy	2.71	0.54	Silty clay loam	0.33	0.67	0.00	0.062
QC-01	Macdonald campus “Beach”	2.73	0.43	Sand	0.02	0.05	0.93	0.015
QC-02	Macdonald campus “Field 9”	2.69	0.48	Loamy sand	0.03	0.17	0.79	0.035
ON-01	Bainsville	2.70	0.43	Silt loam	0.08	0.56	0.37	0.026
ON-02	North Gower	2.76	0.51	Silt loam	0.18	0.75	0.07	0.028
ON-03	Matilda	2.71	0.46	Loamy sand	0.04	0.26	0.71	0.020
ON-04	Uplands	2.76	0.39	Sand	0.01	0.10	0.89	0.014
ON-05	Lyons	2.75	0.38	Sandy loam	0.07	0.37	0.56	0.021
ON-06	Uplands	2.74	0.44	Loamy sand	0.02	0.14	0.84	0.019
ON-07	North Gower	2.76	0.45	Silt loam	0.14	0.54	0.32	0.022
MN-01	Clay loam till (Ryerson series)	2.69	0.55	Silt loam	0.14	0.69	0.17	0.130
MN-02	High lime till (Inwood series)	2.79	0.41	Silt loam	0.24	0.55	0.22	0.300
MN-03	Glaciolacustrine clay (Osborne series)	2.74	0.63	Silt loam	0.21	0.76	0.03	0.130
MN-04	Glaciolacustrine sand (Almassippi ser)	2.71	0.47	Loamy sand	0.03	0.15	0.81	0.035
SK-01	Tarn_01 DWD	2.69	0.41	Silt loam	0.26	0.74	0.00	0.080
SK-02	Tarn_02 GOA	2.70	0.45	Sandy loam	0.06	0.27	0.67	0.018
SK-03	Tarn_03 FXD	2.70	0.53	Silt loam	0.15	0.83	0.02	0.086
SK-04	Tarn_04 AQA	2.68	0.42	Loamy sand	0.03	0.14	0.83	0.015
SK-05	Tarn_05 BRA	2.68	0.45	Sandy loam	0.05	0.28	0.68	0.023
AB-01	Lethbridge	2.64	0.55	Silt loam	0.10	0.52	0.38	0.060
BC-01	FSJ # 1	2.74	0.51	Silty clay	0.42	0.58	0.00	0.087
BC-02	FSJ # 2	2.72	0.50	Silty clay	0.42	0.58	0.00	0.092
BC-03	Vanderhoof	2.71	0.51	Silty clay loam	0.30	0.70	0.00	0.045
BC-04	PG # 1	2.78	0.52	Silty clay	0.41	0.59	0.00	0.086
BC-05	PG # 2	2.77	0.53	Silty clay loam	0.33	0.67	0.00	0.082
BC-06	9718 SW	2.76	0.52	Silt loam	0.10	0.58	0.32	0.058

ρ_s is the density of soil solids ($g \cdot cm^{-3}$)
GSD is soil grain size distribution, i.e., relative proportions of mineral particle sizes; m_{cl}, m_{si}, m_{sa} are fractions of clay, silt, and sand, respectively
LOI is loss on ignition (fraction) at 1050 °C

3 Modeling *Quartz* Content from Measured λ_{sat}

3.1 Theoretical Background

The volumetric content of *quartz* (Θ_{qtz}) can also be assessed from a weighted geometric mean model [9] that generally gives close predictions of λ_{sat}, i.e., soil pore space is completely filled with water:

$$\lambda_{sat-cal} = \lambda_s^{1-n}\lambda_w^n \tag{1}$$

where $\lambda_{sat-cal}$ is the calculated λ_{sat}, λ_w is the thermal conductivity of water, and n is the soil porosity.

The thermal conductivity of water was obtained from experimental data published by Sengers and Watson [11] for $0\,^{\circ}\mathrm{C} \leq T \leq 100\,^{\circ}\mathrm{C}$.

$$\lambda_w = 0.57109 + 0.0017625T - 0.0000067036T^2 \tag{2}$$

Due to simplicity and reliable predictions, the geometric mean model has frequently been used for estimating λ of saturated two-component porous media [7,12]. This model has also been successfully applied to evaluate λ_s,

$$\lambda_s = \lambda_{qtz}^{\Theta_{qtz}}\lambda_{o-min}^{1-\Theta_{qtz}} \tag{3}$$

where λ_{o-min} is the bulk thermal conductivity of all soil minerals excluding *quartz*, assumed to be about $2.0\,\mathrm{W}\cdot\mathrm{m}^{-1}\cdot\mathrm{K}^{-1}$ [7]. For pure *quartz* sands (NS-04), there are no other minerals except *quartz*, so Eq. 3 reduces to $\lambda_s = \lambda_{qtz}$.

In spite of simplicity, Eqs. 1 and 3 are difficult to use due to a lack of Θ_{qtz} and λ_s data. Their real values are unknown and rough estimates of Θ_{qtz} and λ_s result in uncertain model predictions. In spite of this, both parameters can be indirectly assessed from measured λ_{sat} data ($\lambda_{sat-exp}$). Therefore, by combining Eqs. 1 and 3, λ_s and Θ_{qtz} can be calculated (λ_{s-cal} and $\Theta_{qtz-cal}$) from the following relations:

$$\lambda_{s-cal} = \left(\frac{\lambda_{sat-exp}}{\lambda_w^n}\right)^{1/(1-n)} \tag{4}$$

$$\Theta_{qtz-cal} = \frac{\ln(\lambda_{s-cal}/\lambda_{o-min})}{\ln(\lambda_{qtz}/\lambda_{o-min})} \tag{5}$$

Quartz is an anisotropic, trigonal mineral, whose thermal conductivity depends on its crystallographic orientation. At about 15 °C, with heat flow perpendicular ($\perp$) to the optical *c*-axis,$\lambda_{qtz-\perp} = 6.5\,\mathrm{W}\cdot\mathrm{m}^{-1}\cdot\mathrm{K}^{-1}$ whereas for heat flow parallel ($||$) to the optical *c*-axis, $\lambda_{qtz-||} = 11.3\,\mathrm{W}\cdot\mathrm{m}^{-1}\cdot\mathrm{K}^{-1}$ [13]. This mineral has no distinct cleavage and displays no specific orientation. Thus, a bulk thermal conductivity of randomly oriented *quartz* crystals is commonly used and its value is usually assessed

Table 2 Canadian soil minerals and their values of thermal conductivity at ambient T (after Clauser and Huenges [15], Brigaud and Vasseur [16], and Horai [17])

Mineral	$\lambda_{\min}$ ($W \cdot m^{-1} \cdot K^{-1}$)
Quartz (qtz)	7.70
Microcline (mcr)	2.10
Kaolinite (kln)	2.44
Illite (ill)	1.62
Albite (ab)	1.90
Goethite (gt)	2.91
Chlorite (chl)	3.01
Amphibole (am)	2.81
Calcite (cal)	3.03
Dolomite (dol)	5.07
Smectite (sme)	1.73
Hematite (hem)	10.68

by a weighted arithmetic mean [14]:

$$\lambda_{\mathrm{qtz}} = \frac{1}{3}\left(2\lambda_{\mathrm{qtz}-\perp} + \lambda_{\mathrm{qtz}-||}\right) \tag{6a}$$

or by a weighted geometric mean [13]:

$$\lambda_{\mathrm{qtz}} = \lambda_{\mathrm{qtz}-\perp}^{2/3}\lambda_{\mathrm{qtz}-||}^{1/3} \tag{6b}$$

A large majority of predictive λ models assume λ_{qtz} as temperature (T) independent, but in actuality, λ_{qtz}declines with increasing T. This dependence, based on data published by Clauser and Huenges [15] and Eq. 6b, can be described by the following fitted relation:

$$\lambda_{\mathrm{qtz}} = 8.128 - 0.021T\,(0\,^{\circ}\mathrm{C} < T < 100\,^{\circ}\mathrm{C}) \tag{7}$$

The other remaining minerals present in Canadian soils, excluding *hematite* and *dolomite*, have a notably lower thermal conductivity than λ_{qtz} (Table 2).

A bulk value of $\lambda_{\mathrm{o-min}}$ can also be estimated from the extended geometric mean model.

$$\lambda_{\mathrm{o-min-calc}}^{1-\Theta_{\mathrm{qtz}}} = \lambda_{\mathrm{mcr}}^{\Theta_{\mathrm{mcr}}}\lambda_{\mathrm{k\,ln}}^{\Theta_{\mathrm{k\,ln}}}\lambda_{\mathrm{ill}}^{\Theta_{\mathrm{ill}}}\lambda_{\mathrm{ab}}^{\Theta_{\mathrm{ab}}}\lambda_{\mathrm{gt}}^{\Theta_{\mathrm{gt}}}\lambda_{\mathrm{chl}}^{\Theta_{\mathrm{chl}}}\lambda_{\mathrm{am}}^{\Theta_{\mathrm{am}}}\lambda_{\mathrm{cal}}^{\Theta_{\mathrm{cal}}}\lambda_{\mathrm{dol}}^{\Theta_{\mathrm{dol}}}\lambda_{\mathrm{sme}}^{\Theta_{\mathrm{sme}}}\lambda_{\mathrm{hem}}^{\Theta_{\mathrm{hem}}} \tag{8}$$

where $\Theta_{\min}$ is the mineral volumetric fraction of *quartz* or other minerals in the soil sample.

3.2 Measurement of λ_{sat}

Proper preparation of saturated soil samples is essential for obtaining reliable λ_{sat} data [18]. First, a mass of dry soil, equivalent to the assumed dry bulk density, was added to a known volume of a cylindrical container. The required soil compaction was accomplished by repeatedly tapping the lateral surface of the cylindrical container. For all soils, degassed water was gradually added along the cylinder's perimeter until the total mass of added water was equal to the calculated mass of water corresponding to the relative volume (n) needed for saturation of the tested soil. Particular attention was paid to removing trapped air between soil particles; this was a difficult problem in very fine soils (especially clay soils). The saturated soil sample was placed in a laboratory vacuum chamber and exposed to air pressure at 1 mmHg to 10 mmHg to accelerate the removal of trapped air. The λ_{sat} for 40 Canadian soils were measured using a thermal conductivity probe (TCP) that consisted of a stainless steel sheath containing a constantan heater wire and a T-type thermocouple. The internal space of the sheath was filled with a low viscosity epoxy. To simulate a line heat source, the ratio of the probe's length to the probe's diameter was at least 50:1. The allotted heating time for each λ_{sat} measurement was approximately 120 s. For λ_{sat} measurements, the temperature rise of the probe was kept below 4 °C by maintaining a constant current of 0.21 A (supplied to the probe heater) resulting in a TCP source strength of 9.9 W $\cdot$ m^{-1}. The overall uncertainties of λ measurements (relative error) for saturated soils varied from 3 % to 6 %. More details about λ_{sat} measurements can be obtained from Tarnawski et al. [18].

3.3 Reverse Modeling of λ_{o-min}, λ_s, and Θ_{qtz}

It is worth noting that volume fractions of *quartz* (Θ_{qtz}) and other minerals (Θ_{o-min}) must be used in reverse modeling with Eqs. 4, 5, and 8; while from XRF/XRD experiments, mineral contents are usually expressed in mass (weight) percent. Therefore, Θ_{min} was obtained using the following relation:

$$\Theta_{min} = m_{min} \frac{\rho_s}{\rho_{min}} \tag{9}$$

where ρ_s is the bulk density of all minerals comprising a solid phase; ρ_{min} and m_{min} are the bulk density and fractional mass% of *quartz* or other specific minerals.

The density of the solid fraction was measured using a pycnometer method [19]. The densities of soil solids were within (2.665 ± 0.125) g $\cdot$ cm^{-3} (Table 1). Since the density variation is about ± 5 %, for practical applications, the densities of all minerals were generally assumed to be approximately the same ($\rho_{min} \approx \rho_s =$ constant). As a result, the following study will be based on the assumption that $\Theta_{min} = m_{min}$. A summary of soil physical characteristics such as n, λ_{sat}, $\lambda_{o-min-calc}$, λ_{s-cal}, and Θ_{qtz} data are given in Table 3. The reverse modeling approach of λ_{o-min}, λ_s, and Θ_{qtz} proceeds along the following steps: first, the value of $\lambda_{o-min-calc}$ for each soil was obtained using Eq. 8 based on the mineral composition given in the Appendix; second,

the value of λ_{s-calc} for each soil was obtained from Eq. 4 based on the data in Table 3; and third, the *quartz* content for each soil was then calculated using Eq. 5.

Table 3 Summary of reverse modeling of *quartz* content

Code	T (°C)	n (–)	λ_{sat} ($W \cdot m^{-1} \cdot K^{-1}$)	$\lambda_{o-min-calc}$ ($W \cdot m^{-1} \cdot K^{-1}$)	λ_s ($W \cdot m^{-1} \cdot K^{-1}$)	$\Theta_{qtz-XRD/XRF}$ (–)	$\Theta_{qtz-rev-calc}$ (–)	$\Theta_{qtz-rev-ave}$ (–)
NS-01	23	0.55	1.46	1.99	3.95	0.51	0.56	0.54
NS-02	22	0.45	1.93	2.01	4.54	0.61	0.68	0.67
NS-03	22	0.40	2.17	1.96	4.63	0.63	0.70	0.68
NS-04	24	0.36	3.17	–[a]	7.70[a]	1.00	1.03[b]	1.03[b]
NS-05	24	0.40	2.39	2.08	5.29	0.72	0.81	0.81
NS-06	24	0.51	1.76	2.04	4.80	0.65	0.72	0.71
NS-07	24	0.57	1.40	1.95	3.09	0.34	0.57	0.54
PE-01	23	0.44	1.92	2.01	4.85	0.66	0.64	0.63
PE-02	24	0.42	1.94	2.18	4.51	0.58	0.58	0.59
PE-03	24	0.41	1.98	2.16	4.27	0.54	0.58	0.58
NB-01	24	0.54	1.46	2.01	4.30	0.57	0.53	0.50
NB-02	22	0.56	1.35	2.00	4.24	0.56	0.47	0.44
NB-03	24	0.62	1.14	2.10	4.27	0.55	0.32	0.32
NB-04	23	0.54	1.31	2.02	4.49	0.60	0.35	0.32
NB-05	22	0.54	1.46	1.92	3.30	0.39	0.55	0.51
QC-01	23	0.43	1.59	2.06	3.26	0.35	0.36	0.34
QC-02	23	0.48	1.57	2.08	3.59	0.42	0.45	0.45
ON-01	26	0.43	1.60	2.10	3.01	0.28	0.35	0.34
ON-02	23	0.51	1.16	2.01	2.53	0.17	0.08	0.05
ON-03	26	0.46	1.52	2.00	3.45	0.41	0.38	0.35
ON-04	26	0.39	1.67	2.00	3.32	0.38	0.35	0.32
ON-05	26	0.38	1.74	2.17	3.40	0.36	0.34	0.35
ON-06	25	0.44	1.60	2.13	3.45	0.38	0.37	0.37
ON-07	25	0.45	1.46	2.08	2.88	0.25	0.28	0.26
MN-01	25	0.55	1.43	2.70	4.00	0.38	0.38	0.50
MN-02	25	0.41	2.19	3.54	4.13	0.20	0.53	0.72
MN-03	25	0.63	1.05	2.21	2.86	0.21	0.14	0.17
MN-04	25	0.47	1.93	2.44	4.88	0.61	0.70	0.73
SK-01	24	0.41	1.97	2.34	4.12	0.48	0.54	0.58
SK-02	24	0.45	1.73	1.94	4.46	0.61	0.54	0.51
SK-03	23	0.53	1.27	2.29	3.57	0.37	0.20	0.25
SK-04	23	0.42	1.82	1.88	4.80	0.67	0.54	0.50
SK-05	23	0.45	1.84	2.08	4.72	0.63	0.60	0.60
AB-01	22	0.55	1.39	1.99	4.17	0.55	0.48	0.45
BC-01	24	0.51	1.20	2.05	2.70	0.21	0.13	0.10
BC-02	23	0.50	1.21	2.03	2.61	0.19	0.13	0.10
BC-03	23	0.51	1.30	2.02	2.89	0.27	0.27	0.24
BC-04	23	0.52	1.12	2.08	2.60	0.17	0.03	0.01
BC-05	23	0.53	1.14	2.10	2.62	0.17	0.08	0.07

Table 3 continued

Code	T (°C)	n (–)	λ_{sat} ($W \cdot m^{-1} \cdot K^{-1}$)	$\lambda_{o-min-calc}$ ($W \cdot m^{-1} \cdot K^{-1}$)	λ_s ($W \cdot m^{-1} \cdot K^{-1}$)	$\Theta_{qtz-XRD/XRF}$ (–)	$\Theta_{qtz-rev-calc}$ (–)	$\Theta_{qtz-rev-ave}$ (–)
BC-06	24	0.52	1.43	2.10	3.38	0.37	0.42	0.42

[a] Pure *quartz* sands do not contain other minerals; hence, $\lambda_s = \lambda_{qtz}$

[b] Excess values of *quartz* content are probably caused by the experimental error of 3 % to 6 % for λ_{sat}, where λ_s is calculated by Eq. 3, $\Theta_{qtz-XRD/XRF}$ is the measured (XRD/XRF) *quartz* content; $\Theta_{qtz-rev-calc}$ is the calculated *quartz* content (Eq. 5) through the reverse modeling approach using $\lambda_{o-min-calc}$ (Eq. 8) and Table 7; $\Theta_{qtz-rev-ave}$ is the calculated *quartz* content (Eq. 5) through the reverse modeling using an average value of $\lambda_{o-min-ave} = 2.13\ W \cdot m^{-1} \cdot K^{-1}$ (which is the average value of $\lambda_{o-min-calc}$)

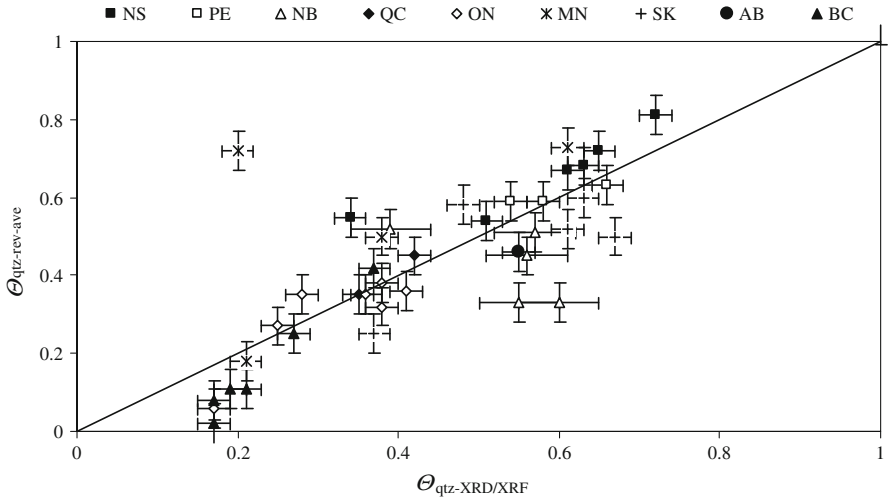

Fig. 1 *Quartz* content: measured ($\Theta_{qtz-XRD/XRF}$) versus reverse modeling ($\Theta_{qtz-rev-ave}$)

Figure 1 illustrates the correlation between the measured and modeled *quartz* contents. In general, *quartz* estimates followed XRD/XRF data sufficiently well. Error bars are within ± 0.05 for $\Theta_{qtz-rev-ave}$ and ±0.02 for $\Theta_{qtz-XRD/XRF}$ except for New Brunswick samples with ±0.05. The results closely overlapped for soils from Ontario (ON), Quebec (QC), Prince Edward Island (PE), and the majority of samples from Nova Scotia (NS), but showed a distinctive disagreement for New Brunswick (NB) soils.

This may be due to difficulties in XRD Rietveld quantification refinements. Soils from New Brunswick are rich in clay minerals which are generally difficult to refine due to their highly variable crystal structure. As a result, only a semi-quantitative analysis was carried out [3].

3.4 Results and Discussion

For the 40 Canadian soils investigated, the average $\lambda_{o-min-ave}(2.13\ W \cdot m^{-1} \cdot K^{-1})$ was slightly higher than $2.0\ W \cdot m^{-1} \cdot K^{-1}$ as proposed by Johansen [7] and it did

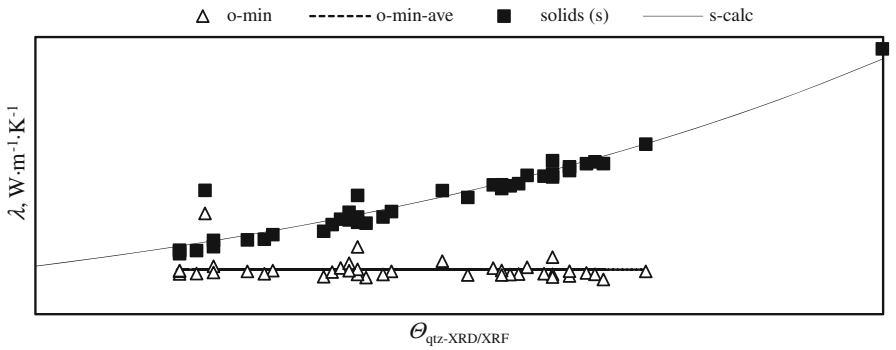

Fig. 2 Thermal conductivity of other minerals ($\lambda_{o-min-calc}$) and solids (λ_{s-calc}) versus $\Theta_{qtz-XRD/XRF}$

not depend on the soil texture. However, a few soils (Fig. 2) had notably higher $\lambda_{o-min-cal}$ values than $2.13\,W \cdot m^{-1} \cdot K^{-1}$, namely: MN-01 ($2.7\,W \cdot m^{-1} \cdot K^{-1}$), MN-02 ($3.54\,W \cdot m^{-1} \cdot K^{-1}$), MN-04 ($2.44\,W \cdot m^{-1} \cdot K^{-1}$), and SK-01 ($2.34\,W \cdot m^{-1} \cdot K^{-1}$). These elevated $\lambda_{o-min-calc}$ values were probably due to the presence of *dolomite* ($5.07\,W \cdot m^{-1} \cdot K^{-1}$) and *calcite* ($3.03\,W \cdot m^{-1} \cdot K^{-1}$). *Quartz* content was estimated by reverse modeling of the geometric mean formula (Eq. 5), using $\lambda_{o-min-calc}$ (Eq. 8) or $\lambda_{o-min-ave} = 2.13\,W \cdot m^{-1} \cdot K^{-1}$; consequently, $\Theta_{qtz-rev-calc}$ and $\Theta_{qtz-rev-ave}$ were obtained, respectively. The differences between $\Theta_{qtz-rev-calc}$ and $\Theta_{qtz-rev-ave}$ were generally insignificant, the only exception were two soils from Manitoba, namely (showing $\Theta_{qtz-rev-calc}$ vs $\Theta_{qtz-rev-ave}$): MN-01 (0.38 vs 0.50) and MN-02 (0.53 vs 0.72). This indicates that $\lambda_{o-min-ave} = 2.13\,W \cdot m^{-1} \cdot K^{-1}$ can be generally applied for estimations of Θ_{qtz} from λ_{sat} data of the 40 Canadian soils.

The thermal conductivity of soil solids was estimated using mineral experimental data (Appendix) with the combination of Eqs. 3 and 8. A strong correlation between λ_s and $\Theta_{qtz-XRD/XRF}$ was obtained (Fig. 5); in a full range of *quartz* content, λ_s varies from $2.2\,W \cdot m^{-1} \cdot K^{-1}$ to $7.6\,W \cdot m^{-1} \cdot K^{-1}$,

$$\lambda_s = \exp\left(0.794 + 1.214\Theta_{qtz}\right) R^2 = 0.953 \tag{10}$$

In terms of reverse modeling of *quartz* occurrence in 40 Canadian soils, its estimates ($\Theta_{qtz-rev-ave}$), based on $\lambda_{o-min-ave} = 2.13\,W \cdot m^{-1} \cdot K^{-1}$, closely followed experimentally obtained data ($\Theta_{qtz-XRD/XRF}$) with a few exceptions. These exceptions (showing $\Theta_{qtz-rev-ave}$ vs $\Theta_{qtz-XRD/XRF}$) were as follows: NS-07 (0.34 vs 0.55), NB-03 (0.55 vs 0.33), NB-04 (0.60 vs 0.33), MN-02 (0.20 vs 0.72), BC-04 (0.17 vs 0.02), and BC-05 (0.17 vs 0.08). A detailed analysis of experimental and modeling data revealed that the thermal conductivity of solids (Eq. 3) was strongly related to $\Theta_{qtz-XRD/XRF}$.

A sensitivity analysis applied to $\Theta_{qtz-rev-ave}$ revealed that their values depended strongly on λ_{sat} data. For a large majority of studied soils, measured λ_{sat} data varied within $\pm 0.1\,W \cdot m^{-1} \cdot K^{-1}$ and had high repeatability; consequently, the overall errors were within 3 % to 6 % [18]. This may partially explain the differences between $\Theta_{qtz-XRD/XRF}$ and $\Theta_{qtz-rev-ave}$. Overall, no straightforward relation between mass

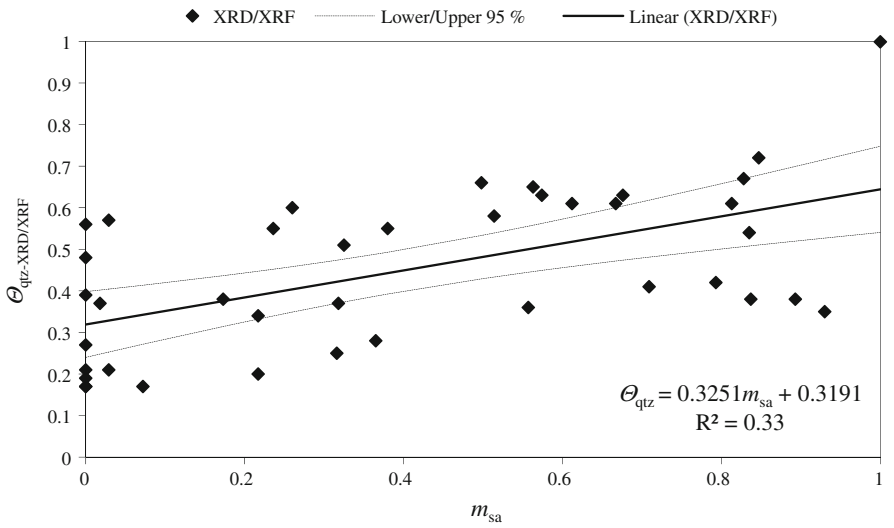

Fig. 3 Measured *quartz* content ($\Theta_{qtz-XRD/XRF}$) versus sand mass fraction

fraction of sand and *quartz* content was observed (Fig. 3). The linear equation given in Fig. 3 indicates that approximately 33 % of the variation in the values of $\Theta_{qtz-XRD/XRF}$ was accounted for by its linear relationship with m_{sa}. The graph contains 95 % confidence limits for the linear equation. The majority of the data were outside the confidence limits, indicating that the linear relationship was not significant.

This outcome could be due to the assumption that *quartz* appeared solely in the coarser textural class of soils (sands). Consequently, this correlation can only provide rough estimates of Θ_{qtz}. A detailed examination of XRD/XRF data, for the 40 Canadian soils, revealed some soils without sand fraction, e.g., NB-02, NB-05, BC-01 to BC-05, but still with noticeable amounts of *quartz*. This resulted in the assumption that *quartz* can occur in both sand and silt fractions, which have grain sizes ranging from 0.05 mm to 2 mm and from 0.002 mm to 0.05 mm, respectively. Close scrutiny of $\Theta_{qtz-XRD/XRF}$ data revealed an improved correlation (Fig. 4) with combined sand and silt mass fractions ($m_{sa} + m_{si}$). Although the correlation in Fig. 4 has a better coefficient of determination than that of Fig. 3, the majority of data was still outside the confidence limits. Also, soils from Quebec and Ontario exhibited noticeably lower $\Theta_{qtz-XRD/XRF}$ versus combined m_{sa} and m_{si}, than soils from the other provinces. These soils had very small fractions of clay and considerable amounts of highly weather resistant *albite* and *microcline* (a *potassium feldspar*). *Quartz*, *albite*, and *microcline* are primary minerals with a dominant presence in Canadian soils. Due to their high hardness (7.0, 6.5, and 6.0, respectively, on the Mohs scale) and a strong resistance to weathering processes, these minerals are mainly present in m_{sa} and m_{si}.

All these observations point to a very diverse soil genesis that depends mainly on geological and climatic conditions. It was also observed that a noticeably different content of *quartz* occurred in soils of very similar texture, but different geological regions (e.g., NS soils vs ON soils). For that reason, it was decided to split the

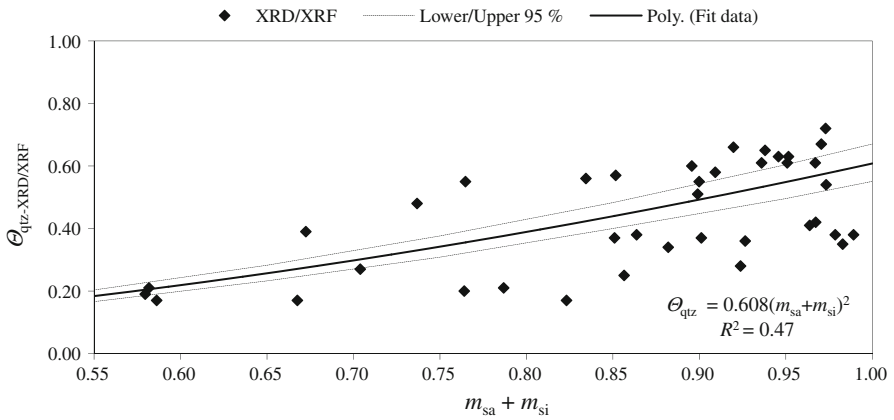

Fig. 4 Measured *quartz* content ($\Theta_{\text{qtz}-\text{XRD/XRF}}$) versus $m_{\text{sa}} + m_{\text{si}}$

Table 4 Fitting coefficients a and b for Eq. 11

Canadian Provinces/Regions	a	b	R^2
NS	−14.72	14.68	0.97
PE–NB	−2.23	1.89	0.91
Eastern (QC–ON)	−8.44	7.59	0.92
Prairie (MN–SK–AB)	−10.06	9.83	0.97
BC	−4.44	3.63	0.93

modeling of *quartz* appearance into five designated regions, namely: NS, PE, and NB, Eastern (QC and ON), Prairie provinces (MN, SK, AB), and BC. These five regions, as well as rough sample locations, can be found in a map of Canada (Appendix). The following fitting relation was obtained for the five regions:

$$\Theta_{\text{qtz}-\text{fit}} = \exp\left[a + b(m_{\text{sa}} + m_{\text{si}})^{0.5}\right] \tag{11}$$

Fitting coefficients a and b are given in Table 4.

Figures 5, 6, 7, 8, and 9 show $\Theta_{\text{qtz}-\text{XRD/XRF}}$ and $\Theta_{\text{q}-\text{fit}}$ versus $(m_{\text{sa}} + m_{\text{si}})$ for the five assigned regions; a slightly diverse $\Theta_{\text{q}-\text{fit}}$ is observed for NS-07, PE-03, SK-01, MN-02, MN-03, and BC-06. The graphs also contain 95 % confidence limits for the fitted relation of Eq. 11. The majority of the data was within the confidence limits.

The *quartz* occurrence in m_{sa} and m_{si} can also be modeled explicitly using the following bi-linear relation which assumes individual contribution of sand and silt fractions:

$$\Theta_{\text{qtz}-\text{fit}} = \xi m_{\text{sa}} + \zeta m_{\text{si}} \tag{12}$$

where ξ and ζ are *quartz* occurrence coefficients for m_{sa} and m_{si}, respectively.

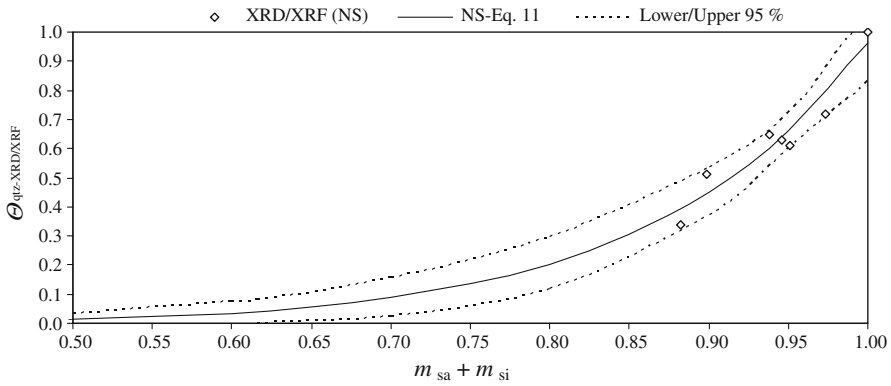

Fig. 5 Measured and predicted *quartz* fraction versus the combined fraction of sand and silt in Nova Scotia (NS)

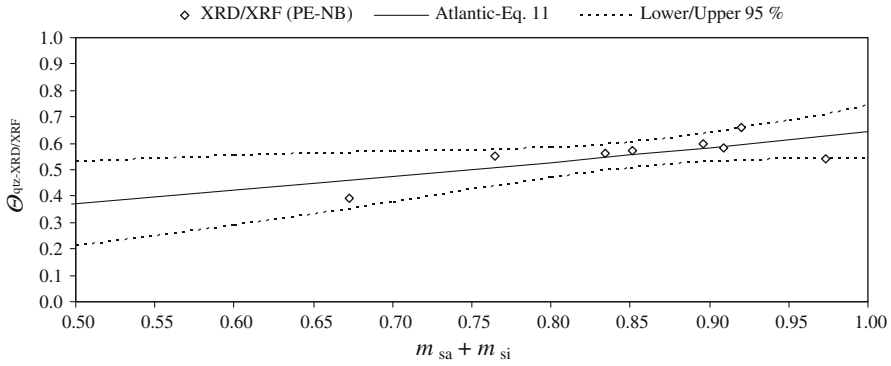

Fig. 6 Measured and predicted *quartz* fraction versus the combined fraction of sand and silt in New Brunswick (NB) and Prince Edward Island (PE)

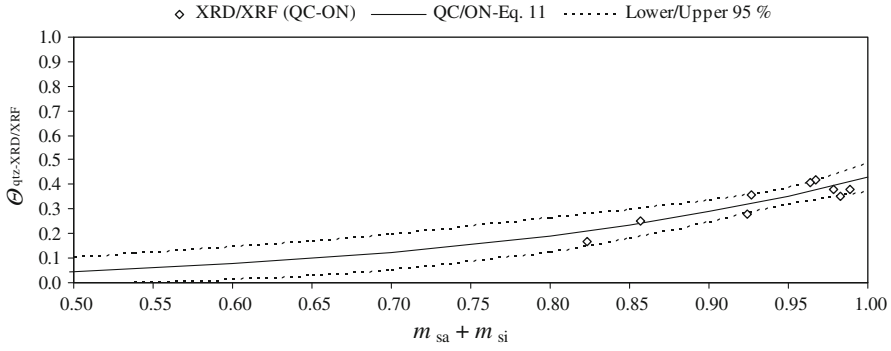

Fig. 7 Measured and predicted *quartz* fraction versus the combined fraction of sand and silt in the Eastern Canadian regions (QC and ON)

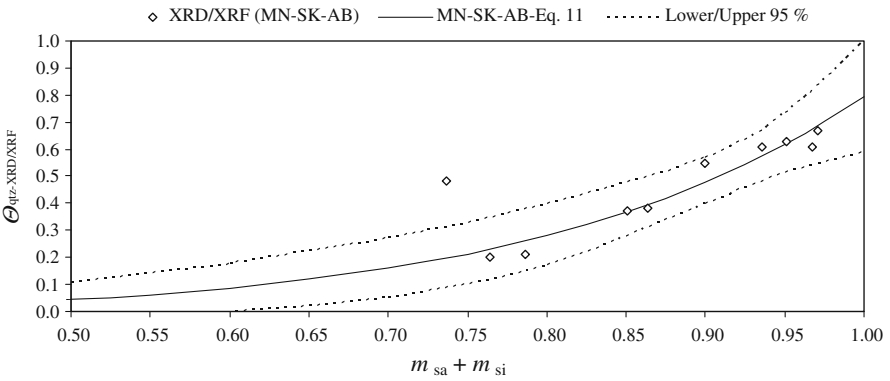

Fig. 8 Measured and predicted *quartz* fraction versus the combined fraction of sand and silt in the Prairie Regions (MN, SK, and AB)

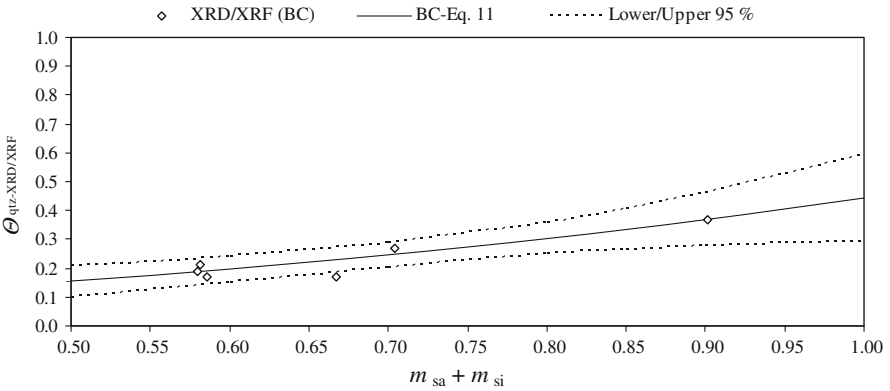

Fig. 9 Measured and predicted *quartz* fraction versus the combined fraction of sand and silt in British Columbia (BC)

The modeling procedure assumed that *quartz* occurred mainly in m_{sa}; contribution from m_{si} took place when $m_{sa} < \Theta_{qtz-XRD/XRF}$. A summary of this procedure is given in Table 5.

Table 5 Contribution of *quartz* from sand and silt fractions

m_{sa} versus $\Theta_{qtz-XRD/XRF}$	ξ	ζ
$m_{sa} > \Theta_{qtz-XRD/XRF}$	$0 < \xi < 1$	$\zeta = 0$
$m_{sa} = \Theta_{qtz-XRD/XRF}$	$\xi = 1$	$\zeta = 0$
$m_{sa} < \Theta_{qtz-XRD/XRF}$	$\xi = 1$	$0 < \zeta < 1$
$m_{sa} = 0$	$\xi = 1$	$0 < \zeta < 1$

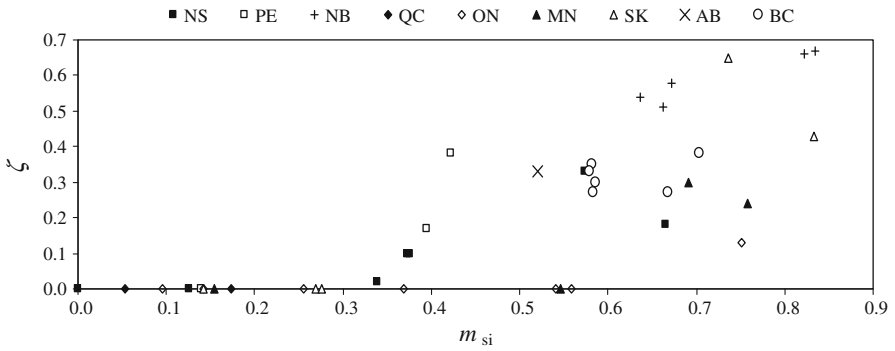

Fig. 10 *Quartz* occurrence coefficient in silt fractions (ζ)

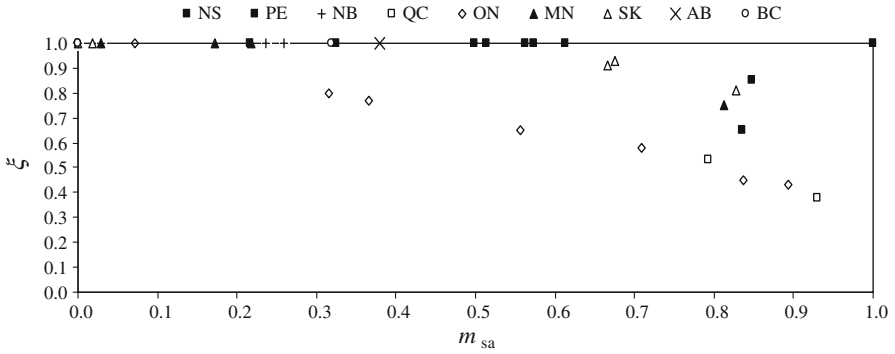

Fig. 11 *Quartz* occurrence coefficient (ξ) in sand fractions

According to the procedure in Table 5, the *quartz* occurrence coefficients were obtained and shown in Figs. 10 and 11. Figure 10 displays no *quartz* occurrence ($\zeta = 0$) in soils having low fractions of silt ($0 < m_{si} < 0.34$), then ζ increases randomly to 0.67. The coefficient of *quartz* occurrence in sand fractions (ξ) is shown in Fig. 10.

From Figs. 10 and 11 it is shown that the coefficients are widely scattered; however, they show better correlation when the data are split into five regions as before, namely: NS, PE, and NB, Eastern (QC and ON), Prairie (MN, SK, and AB) provinces, and BC. For NS, PE, and NB), the following ζ relation is obtained:

$$\zeta = m_{si}^2 \quad R^2 = 0.82 \tag{13}$$

Soil samples from the Eastern provinces (QC and ON) do not have any *quartz* in silt fractions, with the exception of a sample from North Gower. Therefore, the following $\zeta = 0$ was assumed; $\zeta = 0.13$ for North Gower was ignored.

Samples from the Prairie provinces (MN, SK, AB) only contain *quartz* at higher fractions of silt ($m_{si} > 0.54$); then, an increasing ζ trend was observed. For the Prairie provinces, the following ζ relation is obtained:

$$\zeta = 0.01 + 0.877 m_{si}^3 \quad R^2 = 0.65 \tag{14}$$

For BC, the following ζ relation is obtained.

$$\zeta = 0.403 m_{si}^{0.5} \qquad R^2 = 0.90 \tag{15}$$

In turn, the coefficient of *quartz* occurrence in sand fractions (ξ) remains constant with m_{sa} for the majority of soils from the Atlantic provinces, except for NS-06 ($\xi = 0.85$) and PE-03 ($\xi = 0.65$). Therefore, these values were ignored and $\xi = 1$ was used.

For the Eastern (Eq. 16) and Prairie provinces (Eq. 17) and also for BC (Eq. 18) strong correlations are observed and they are given, respectively, as follows:

$$\xi = 1.03 - 0.68 m_{sa} \qquad R^2 = 0.98 \tag{16}$$

$$\xi = 1 - 0.382 m_{sa}^3 \qquad R^2 = 0.93 \tag{17}$$

$$\xi = 1 \qquad R^2 = 1 \tag{18}$$

Table 6 summarizes *quartz* measurements versus predictions made by Eqs. 11 and 12 with the *quartz* occurrence coefficients given by Eqs. 13–18. Two approaches for modeling *quartz* content were evaluated with respect to experimental data of $\Theta_{q-XRD/XRF}$ using the root-mean-squared error (RMSE):

$$\mathrm{RMSE} = \sqrt{\frac{1}{N}\sum_{1}^{N}\left(\Theta_{qtz-XRD/XRF} - \Theta_{qtz-calc}\right)^2} \tag{19}$$

where $\Theta_{qtz-XRD/XRF}$ represents experimental data; $\Theta_{qtz-calc}$ represents predicted data (Eqs. 11 or 12), and N is the number of recorded experimental data.

Generally, *quartz* predictions (using Eqs. 11 and 12) satisfactorily follow experimental data with RMSE of ± 0.06 and ± 0.08, respectively. Modeling the *quartz* content, by Eq. 12, is more cumbersome; for that reason, the use of Eq. 11 is recommended.

Table 6 Comparison of measured and predicted Θ_{qtz} data

Sample code	$m_{si} + m_{sa}$	$\theta_{q-XRD/XRF}$	$\theta_{qtz-Eq.11}$	θ_{q-Eq12}
NS-01	0.899	0.51	0.45	0.44
NS-02	0.951	0.61	0.67	0.64
NS-03	0.946	0.63	0.64	0.61
NS-04	1.000	1.00	0.96	1.00
NS-05	0.973	0.72	0.79	0.85
NS-06	0.938	0.65	0.61	0.60
NS-07	0.882	0.34	0.39	0.40
PE-01	0.920	0.66	0.60	0.61

Table 6 continued

Sample code	$m_{si} + m_{sa}$	$\theta_{q-XRD/XRF}$	$\theta_{qtz-Eq.11}$	$\theta_{q-Eq.12}$
PE-02	0.909	0.58	0.59	0.61
PE-03	0.973	0.54	0.63	0.84
NB-01	0.852	0.57	0.56	0.61
NB-02	0.834	0.56	0.55	0.60
NB-03	0.765	0.55	0.51	0.44
NB-04	0.896	0.60	0.58	0.57
NB-05	0.672	0.39	0.46	0.35
QC-01	0.983	0.35	0.40	0.37
QC-02	0.967	0.42	0.38	0.39
ON-01	0.924	0.28	0.32	0.29
ON-02	0.823	0.17	0.21	0.07
ON-03	0.964	0.41	0.37	0.39
ON-04	0.989	0.38	0.41	0.38
ON-05	0.927	0.36	0.32	0.36
ON-06	0.979	0.38	0.39	0.39
ON-07	0.856	0.25	0.24	0.26
MN-01	0.864	0.38	0.40	0.38
MN-02	0.764	0.20	0.23	0.30
MN-03	0.787	0.21	0.26	0.33
MN-04	0.967	0.61	0.67	0.65
SK-01	0.737	0.48	0.20	0.27
SK-02	0.936	0.61	0.58	0.60
SK-03	0.851	0.37	0.37	0.45
SK-04	0.971	0.67	0.69	0.65
SK-05	0.952	0.63	0.62	0.60
AB-01	0.900	0.55	0.48	0.44
BC-01	0.582	0.21	0.19	0.17
BC-02	0.580	0.19	0.19	0.17
BC-03	0.704	0.27	0.25	0.25
BC-04	0.586	0.17	0.19	0.18
BC-05	0.668	0.17	0.23	0.23
BC-06	0.901	0.37	0.37	0.49
		RMSE	0.06	0.08

4 Conclusions and Recommendations

The measured mineral composition data (XRD/XRF) of 40 Canadian soils were modeled for the presence of *quartz* as a function of soil texture. The analysis of preliminary modeling revealed a lack of strict correlation between *quartz* content and mass fraction of sand, as previously suggested by Peters-Lidard et al. [5] and modeled by Tarnawski

et al. [9], for a limited number of soils. For that reason, the occurrence of *quartz* content was modeled as dependent on a combined fraction of sand and silt, which produced an improved correlation for the 40 tested soils. However, it was noted that a noticeably different content of *quartz* occurred in soils of very similar texture, but different origins (e.g., NS soils vs ON soils). Consequently, based on the fact that soil mineralogy is strongly influenced by climatic factors and the parent material from which soils are formed, all soils were modeled separately for five assigned regions. As a result, good correlations of *quartz* versus combined sand and silt fractions were obtained. Soils from Quebec and Ontario exhibited noticeably lower *quartz* occurrence than analyzed soils from the other provinces. This outcome may be due to considerable amounts of highly weather resistant *albite* and moderately weather resistant *K-feldspar* (*microcline*). Generally, *quartz* predictions (using Eqs. 11 and 12) satisfactorily follow experimental data with RMSE of ± 0.06 and ± 0.08, respectively. Modeling the *quartz* content, by Eq. 12, is more cumbersome; for that reason, the use of Eq. 11 is recommended.

Estimates of *quartz* content and an average thermal conductivity of other minerals were also obtained by the reverse analysis of the weighted geometric mean model applied to the experimental thermal conductivity data of saturated soils. The thermal conductivity of the remaining soil minerals was about $2.13\,\mathrm{W \cdot m^{-1} \cdot K^{-1}}$ on average and did not depend on the soil texture.

In general, *quartz* content estimates obtained by the reverse analysis of thermal conductivity data at full saturation were comparable with the XRD/XRF data. This proves that satisfactory estimates of *quartz* content can be indirectly obtained from soil thermal conductivity measurements at full saturation under conditions of very careful soil sample preparation and high measurement accuracy.

Acknowledgments This work was supported by Discovery Grants from Natural Sciences and Engineering Research Council (NSERC) Canada. Sincere thanks are expressed to the Geological Survey of Bavaria (Germany) for providing XRD/XRF analyses and to all the soil samples suppliers from the Canadian provinces mentioned.

Appendix

See Table 7 and Fig. 12.

Table 7 Mineral composition of Canadian soils (mass%)

Code	*Quartz*	*K-Feldspar (Microcline)*	*Kaolinite*	*Illite*	*Albite*	*Goethite*	*Fe-Chlorite*	*Amphibole*	*Calcite*	*Dolomite*	*Smectite*	*Hematite*
NS-01	51	2	5	20	13	4	5	–	–	–	–	–
NS-02	61	4	2	15	10	2	6	–	–	–	–	–
NS-03	60	4	4	15	9	2	3	–	–	–	–	–
NS-04	100	–	–	–	–	–	–	–	–	–	–	–
NS-05	72	12	–	6	5	–	5	–	–	–	–	–
NS-06	65	10	3	12	4	3	3	–	–	–	–	–
NS-07	34	13	4	32	7	7	3	–	–	–	–	–
PE-01	66	9	2	14	3	2	4	–	–	–	–	–
PE-02	58	8	3	12	11	–	6	–	–	–	–	2
PE-03	54	16	2	12	9	–	5	–	–	–	–	2
NB-01	57	2	5	16	12	3	5	–	–	–	–	–
NB-02	56	1	4	15	16	3	5	–	–	–	–	–
NB-03	55	6	5	11	13	3	7	–	–	–	–	–
NB-04	60	3	4	15	10	3	5	–	–	–	–	–
NB-05	39	1	3	34	11	5	7	–	–	–	–	–
QC-01	35	12	–	–	43	–	4	6	–	–	–	–
QC-02	42	13	–	5	29	–	7	4	–	–	–	–
ON-01	28	14	–	6	36	1	7	8	–	–	–	–
ON-02	17	8	–	19	39	3	5	9	–	–	–	–
ON-03	41	10	–	4	38	–	–	7	–	–	–	–
ON-04	38	12	–	4	39	–	–	7	–	–	–	–
ON-05	36	12	–	–	35	–	8	9	–	–	–	–
ON-06	38	10	–	–	38	–	10	4	–	–	–	–

Table 7 continued

Code	*Quartz*	*K-Feldspar (Microcline)*	*Kaolinite*	*Illite*	*Albite*	*Goethite*	*Fe-Chlorite*	*Amphibole*	*Calcite*	*Dolomite*	*Smectite*	*Hematite*
ON-07	25	15	–	9	35	–	7	9	–	–	–	–
MN-01	38	8	8	7	10	3	3	–	10	13	–	–
MN-02	20	3	2	2	8	–	–	–	28	37	–	–
MN-03	21	–	8	25	8	5	7	–	10	5	11	–
MN-04	61	7	3	1	15	–	4	2	2	5	–	–
SK-01	48	7	2	8	17	2	2	–	9	5	–	–
SK-02	61	5	2	10	19	1	2	–	–	–	–	–
SK-03	37	10	9	11	13	3	7	–	8	2	–	–
SK-04	67	4	–	10	17	–	–	2	–	–	–	–
SK-05	63	7	4	6	14	2	4	–	–	–	–	–
AB-01	55	5	4	16	13	3	4	–	–	–	–	–
BC-01	21	–	11	35	13	7	13	–	–	–	–	–
BC-02	19	–	11	38	13	8	11	–	–	–	–	–
BC-03	27	10	5	14	34	4	6	–	–	–	–	–
BC-04	17	8	13	28	16	7	11	–	–	–	–	–
BC-05	17	9	11	27	16	6	14	–	–	–	–	–
BC-06	37	7	4	10	28	5	7	2	–	–	–	–

Fig. 12 Canadian provinces and their assigned regions showing rough sample locations (modified from [3])

References

1. B.L. Allen, B.F. Hajek, in *Minerals in Soil Environments*, ed. by J.B. Dixon, S.B. Weed (Soil Science Society of America, Madison, WI, 1989), p. 200
2. J.B. Rowse, W.B. Jepson, J. Therm. Anal. **4**, 1969 (1972)
3. J. Schönenberger, T. Momose, B. Wagner, W.H. Leong, V.R. Tarnawski, Int. J. Thermophys. **33**, 342 (2012)
4. M.S. Kersten, Thermal Properties of Soils, Bulletin No. 28 (University of Minnesota, 1949)
5. C.D. Peters-Lidard, E. Blackburn, X. Liang, E.F. Wood, J. Atmos. Sci. **55**, 1209 (1998)
6. D.A. de Vries, in *Physics of the Plant Environment*, ed. by W.R. Van Wijk (Wiley, New York, 1963), p. 210
7. O. Johansen, *Thermal Conductivity of Soils* (Ph.D. Thesis, Trondheim, Norway, 1975) (trans: CRREL, 1977)
8. F. Gori, in *Proceedings of the 4th International Conference on Permafrost* (Fairbanks, Alaska, National Academy Press, Washington, DC, 1983), p. 363
9. V.R. Tarnawski, T. Momose, W.H. Leong, Géotechnique **59**, 331 (2009)
10. S. Lu, T. Ren, Y. Gong, R. Horton, Soil Sci. Soc. Am. J. **71**, 8 (2007)
11. J.V. Sengers, J.T.R. Watson, J. Phys. Chem. Ref. Data **15**, 1291 (1986)
12. M. Woodside, J.M. Messmer, J. Appl. Phys. **32**, 1688 (1961)
13. O.T. Farouki, *Thermal Properties of Soils* (Trans Tech Publications, Switzerland, 1986)
14. D.A. de Vries, Mededelingen van de Landbouwhogeschool te Wageningen **52**, 1 (1952) (trans: Building Research Station, England, Library Communication No. 759)

15. C. Clauser, E. Huenges, in *Rock Physics and Phase Relations, A Handbook of Physical Constants*, ed. by T.J. Ahrens (American Geophysical Union, Washington, 1995), p. 105
16. F. Brigaud, G. Vasseur, Geophys. J. Int. **98**, 525 (1989)
17. K. Horai, J. Geophys. Res. **76**, 1278 (1971)
18. V.R. Tarnawski, W.H. Leong, T. Momose, Int. J. Thermophys. **32**, 984 (2011)
19. B.R. Blake, K.H. Hartge, in *ASA Monograph No. 9*, Part 1, ed. by A. Klute (American Society of Agronomy, Madison, WI, 1986), p. 377